Supplemental Material for BIG-Net: Deep Learning for Grasping with a Bio-Inspired Soft Gripper

Hui Zhang *, Yanming Wu, Eric Demeester, and Karel Kellens

Email: hui.zhang{AT}kuleuven.be

1. Simulator and hardware configuration

Table 1. Main parameters and their descriptions in the simulation

Parameter	Description	Value (metric)
$r_{\mathcal{G}}$	Head radius of gripping pad	10.0 mm
$R_{\mathcal{G}}$	Bottom radius of gripping pad	17.5 mm
H	Altitude of gripping pad	30.0 mm
Δ_θ	Radius step	0.1π rad
Δ_d	Distance step	2.0 mm
(h_i, w_i)	Size of depth image	(240, 240) pixels
$(h_{\mathcal{T}}, w_{\mathcal{T}})$	Size of table	(350, 350) mm
$f_{\mathcal{C}}$	Focal length of camera	525 mm
$N_{\mathcal{O}}$	Maximum number of objects in a grasp scene	20

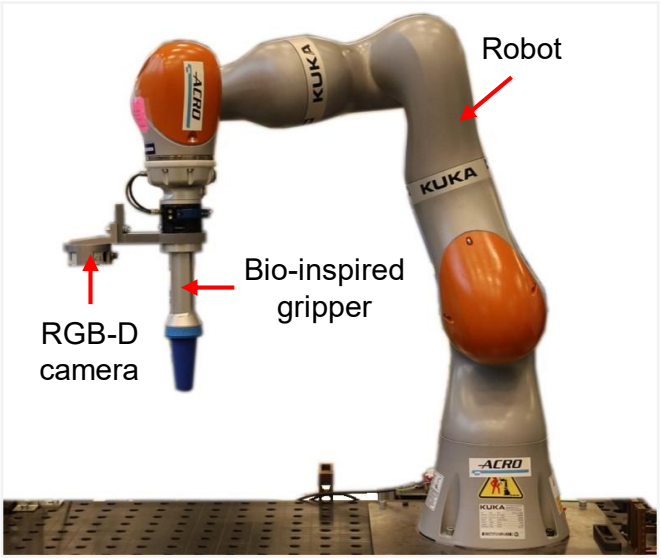

Fig. 1 Robotic setup for the experiments.

2. Verification of the contact model

This section aims to verify the feasibility and robustness of the contact model proposed in the paper. The verification experiments were implemented using the robotic setup mentioned in Section 1 without the RGB-D camera.

The real-time forces on the gripper base are measured by the sensors embedded in the robotic joints. p_{in} = 0.1 bar was configured for the following tests.

A series of benchmarking objects with various shapes were printed by a 3D printer with the polylactic acid (PLA) filament, which are divided into two categories in Fig. 2. Specifically, the objects in Fig. 2 (a) are composed of cylindrical non-airtight tubes, while the objects in Fig. 2 (b) consist of cylindrical airtight surfaces. The 3D-printed objects are fixed on the table, then the gripper ties to approach and pick up the objects with a top-down grasp direction $\boldsymbol{d}_r$ and a pre-defined gripping step s_r. p_{air} = 0 bar is conducted when the gripper grasps an object in Fig. 2 (a), which simplifies the calculation of μ during the subsequent tests.

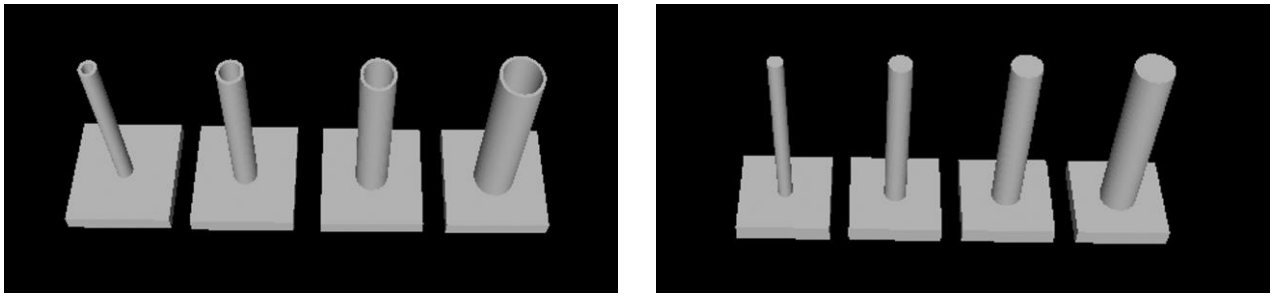

(a) (b)

Fig. 2. Benchmark objects for the verification of the contact model. (a) A set of benchmarking objects with non-airtight surfaces (tubes). (b) A set of benchmarking objects with airtight surfaces.

First, several benchmark objects were grasped to measure the air pressure differential p_{air} between the gripping pad and the atmosphere, and the coefficient of friction μ between the gripper and the object. The 3D-printed objects are fixed on the table, then the gripper tries to approach and pick up the objects with a top-down grasp direction, as shown in Fig. 3. For the used gripper and benchmarking objects printed by the PLA filament, p_{air} = 0.445 bar and μ = 0.99 are computed in ten grasping trials, which are applied to estimate F_z for the subsequent verification tests. Notably, $p_{air} < 1.0$ bar is reported, since the 3D-objects printed by a Laminated Object Manufacturing (LOM) 3D-printer with stiff filaments are not entirely airtight.

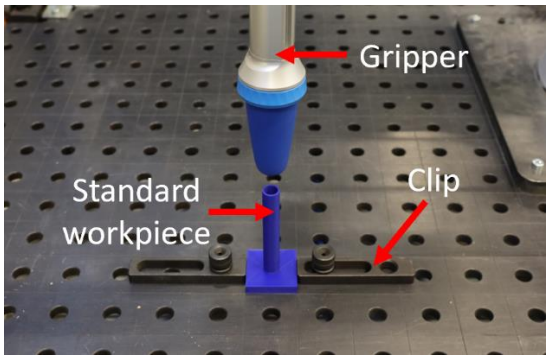

Fig.3 Physical grasping for the verification of the contact model.

Table 2 presents the grasp parameters and gripping forces for eight grasping trials with the objects in Fig. 2 (a). In this table, the simulated F_z is computed based on Eq. (9) - Eq. (12) in the paper, and the real F_z is measured by the embedded force-torque sensors in the robot. Similarly, Table 3 shows the grasp parameters and gripping forces for eight grasping trials with the objects in Fig. 2 (b). The results acquired from Table 2 and Table 3 indicate that the simulated and real value of F_z for each grasping trial are similar. The proposed contact model

performs the F_z estimation with an average error of 0.74 N. Especially, it reports an average error of 0.28 N when $r_c \leq 8.0$ mm.

As a conclusion, the proposed contact model can follow feasible grasp principles and estimate the gripping force with a relatively high accuracy for the bio-inspired soft gripper, which is helpful for the grasp quality estimation in the simulation.

Table 2. Results of the verification tests with the objects in Fig. 2 (a)

r_c (mm)		4.0	4.0	6.0	6.0	8.0	8.0	10.0	10.0
s_r (mm)		15.0	25.0	15.0	25.0	15.0	25.0	15.0	25.0
F_z (N)	Sim.	3.73	6.22	5.60	9.34	7.47	12.45	9.34	15.56
	Real	3.80	6.00	5.22	8.78	7.68	13.00	7.42	13.63
	Error	0.07	0.22	0.38	0.56	0.21	0.55	1.92	1.83

Note: 1) "Sim." is the abbreviation of "Simulated". 2) r_c is the radius of the cylinder on a benchmarking object in Fig. 2.

Table 3. Results of the verification tests with the objects in Fig. 2 (b)

r_c (mm)		4.0	4.0	6.0	6.0	8.0	8.0	10.0	10.0
s_r (mm)		15.0	25.0	15.0	25.0	15.0	25.0	15.0	25.0
F_z (N)	Sim.	5.97	8.46	10.64	14.37	16.42	21.40	23.33	29.55
	Real	6.03	8.38	10.50	13.83	16.94	22.04	21.88	26.79
	Error	0.03	0.11	0.19	0.60	0.42	0.64	1.45	2.76

3. Objects and clutters for the real-world grasping

(a) (b) (c)

Fig. 4. Objects and clutters used for robotic grasping experiments. (a) Part of the used household items. (b) Part of the used adversarial items. (c) A set of stacked objects with random poses.

4. Failure modes in the real-world grasping tests

Failure cases and limitations of the BIG-Net grasping method have to be mentioned.

Fig. 5 (a)-(b) present two failure grasp cases for the grasping of simple objects. Specifically, Fig. 5 (a) reports a failed grasping trial for a tiny and smooth object. The object slips out of the gripping pad during the grasping, since the grasp direction estimated via the BIG-Net is not entirely vertical. Grasp direction constraints are

necessary for the control strategy of the proposed grasping method to grasp tiny and smooth objects. Fig. 5 (b) shows another occasional failure grasping trial for a rather simple object. The BIG-Net detects a "feasible" grasp region with the highest grasp quality q at the center of the object. However, a soft stalk exists in this grasp region. The stalk is too short to be wrapped by the gripping pad but inhibits the gripping pad from wrapping the main body of the object, leading to a lack of gripping force on the contact surface. Once a failed grasp is detected, the BIG-Net grasping method can adjust the grasp strategies and priorities to avoid a failed grasp on the same region, as presented in our previous work [1]. For example, the restrictions of grasp direction and height are adjusted, and the available grasp regions are updated for the following grasping trail in the proposed grasping method. Hence, a successful grasp in Fig. 5 (c) is performed when the system adjusts the grasp strategies after the failed grasp in Fig. 5 (b).

Moreover, Fig. 5 (d)-(e) demonstrate two failure modes with the objects besides the testing dataset, which are relatively complex for the chameleon-tongue inspired gripper. First, Fig. 5 (d) shows a failed grasping trial for a flat and non-airtight object. In such a case, the object cannot be wrapped by the gripper due to the flat surface but could be grasped by F_{vac}. Hence, a "feasible" grasp pose at the center of the object surface is detected via the BIG-Net. Nevertheless, the gripping pad fails to generate an airtight contact surface on the non-airtight object. Second, it is difficult to grasp soft, long and slim objects, such as ropes and USB cables in Fig. 5 (e), with the used bio-inspired gripper. The BIG-Net cannot estimate the grasp direction and wrap the object, attributed to the limitation of the used gripper and inaccurate depth image from the camera.

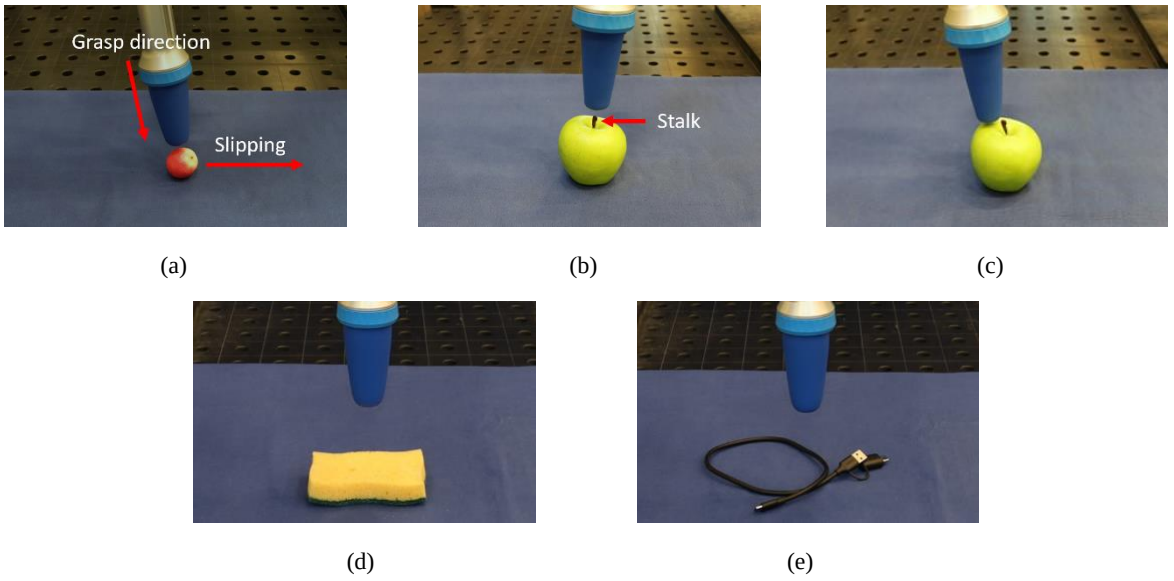

Fig. 5. Failure modes of the BIG-Net grasping method. (a) Grasping a tiny and smooth object. (b) Grasping an object with a short stalk. (c) Grasping the object in subfigure (b) with constrained grasp regions. (d) Grasping a piece of sponge. (e) Grasping a USB cable.

References

[1] Zhang, H., Peeters, J., Demeester, E. and Kellens, K., 2021. A CNN-based grasp planning method for random picking of unknown objects with a vacuum gripper. *Journal of Intelligent & Robotic Systems*, 103(4), pp.1-19.